Pore-Suspending Lipid Bilayers on Porous Alumina Investigated by Electrical Impedance Spectroscopy

Janine Drexler and Claudia Steinem*

Institut für Analytische Chemie, Chemo- und Biosensorik, Universität Regensburg, 93040 Regensburg, Germany

Received: June 17, 2003

Nonordered and ordered porous alumina substrates with pore diameters of 20 and 50 nm, respectively, were utilized to immobilize lipid membranes spanning the pores of the porous material. The substrates were characterized by means of interferometry and electrical impedance spectroscopy. For impedance data reduction, an equivalent circuit representing the electrical behavior of porous alumina was developed on the basis of the parallel layer model. It turned out that the electrical parameters of the as prepared alumina substrates prevent a sensitive monitoring of the formation of immobilized lipid membranes. Thus, we established a technique to modify the substrates with respect to their electrical properties, leading to a significantly increased capacitance of porous alumina, which allowed for a sensitive detection of pore-spanning lipid bilayers by impedance spectroscopy. Two different membrane preparation techniques based on vesicle spreading were investigated. First, negatively charged giant liposomes were spread onto the porous alumina surface under an applied dc voltage of +100 mV. Second, large unilamellar vesicles containing lipids bearing a thiol anchor were used to chemisorb on gold functionalized porous alumina substrates and subsequently rupture to form planar pore-spanning membranes. For both techniques, impedance spectra were obtained, which indicate the formation of lipid bilayers on top of the porous alumina substrates.

Introduction

Solid supported membranes (SSMs) as well as black lipid membranes (BLMs) are established model systems to investigate basic physical properties of lipid bilayers and membrane-confined proteins. Particularly, SSMs have been studied over recent years as a promising tool for constructing biosensors. Owing to their high long term stability and their amenability to sensitive surface analysis tools such as scanning probe microscopy, ATR infrared spectroscopy, the quartz crystal microbalance technique, and surface plasmon resonance spectroscopy, SSMs enable one to rationally design biosensor devices based on sophisticated micromachined chip technology.[1−8] However, it turned out that the suitability of SSMs is restricted by their close surface proximity (typically 0.2−2 nm) that limits or even prevents incorporation of large membrane-spanning proteins and the establishment of chemical and electrochemical transmembrane gradients. These problems can be circumvented using black lipid membranes first established by Müller and Rudin.[9] BLMs allow in principle the incorporation of functional transmembrane proteins; they lack, however, long term stability and are thus not suited for biosensor applications.

To combine the merits of both membrane systems, SSMs and BLMs, we followed a new strategy based on lipid membranes suspending pores of a porous matrix. In this system, membranes anchored to the upper surface of the porous material resemble SSMs, while pore suspending regions can be viewed as nano-BLMs. Recently, we have described a procedure that allows in principle the preparation of pore-suspending bilayers on porous alumina surfaces by a vesicle spreading technique. By means of scanning force microscopy, we were, for the first time, able to visualize these membranes and characterize their mechanical stability.[10,11]

* To whom correspondence should be addressed. Telephone: +49 941 943 4547/4548. Fax: +49 941 943 4491. E-mail: claudia.steinem@chemie.uni-regensburg.de.

To investigate ion transport across suspended membranes, electrically insulating lipid bilayers are required. By means of electrical measurements, the insulating properties of such membranes can be obtained. In this paper, we describe the investigation and modification of porous alumina substrates and pore-suspending lipid membranes by means of electrical impedance spectroscopy. Impedance spectroscopy provides comprehensive information about the dominant electrical processes of the system under investigation. Impedance data are generally discussed in terms of equivalent circuits mostly consisting of parallel and series combinations of ohmic resistances and capacitances. For porous alumina, various models have been proposed to represent its electrical impedance behavior. Early studies of Hoar and Wood[12] described an equivalent circuit consisting of a parallel circuit of a capacitance and an ohmic resistance resembling the Al_2O_3 pore columns, which is in parallel with a parallel circuit of a capacitance and a resistance and in series with an ohmic resistance representing the Al_2O_3 barrier layer at the pore bottoms and the pores filled with electrolyte, respectively. Hoar and Wood argued that the capacitance and ohmic conductance of the Al_2O_3 pore columns are so small that they cannot be detected in the observed frequency range, and hence, the equivalent circuit is reduced by these two elements. For calculating area-related specific parameters, they used the geometric area of the porous alumina exposed to the aqueous phase. The model of Hoar and Wood was adopted by Mansfeld and Kendig[13] for the investigation of anodizing layers. Hitzig et al.[14] proposed a model considering two separate oxide phases, an Al_2O_3 barrier layer at the bottom of the pores and a pore-containing Al_2O_3 layer. Each oxide layer is characterized by a parallel connection of an ohmic resistance and a capacitance. They anticipated that the electrical properties of the two oxide layers can be distinguished and that both can be treated as separate quasi-homogeneous oxide phases. Vereecken and co-workers[15,16] described an equivalent circuit composed

10.1021/jp030762r CCC: $25.00
Published on Web 09/16/2003

of a constant phase element (cpe) instead of a capacitance and an ohmic resistance connected in series. In the case of ideally polarizable electrodes, the presence of a cpe is discussed in terms of surface roughness,[17,18] specific anion adsorption, effects of the solvent, and electrode potential.[19,20] De Levie[21] and Scheider[22] addressed the dispersion phenomenon in terms of infinitely long, branched ladder-networks of capacitances and resistances. Different degrees of branching lead to different values of the index *n*.[15] Vereecken and co-workers[15,16] concluded that information about pore size, volume, and thickness cannot be obtained directly from electrical impedance spectroscopy; only the barrier layer at the bottom of the pores is measured. The main problem is that the active area of the porous alumina surface that was used for calculating area-related specific parameters was not explicitly given.

To obtain lipid membrane specific parameters that can be compared with literature values, the actual measured area of the lipid bilayer is, however, absolutely required. Our objective was to elucidate whether only the area of the pore suspending part of the lipid bilayer is measured or whether the entire lipid membrane covering the top of the porous alumina substrate needs to be taken into account. In this study, we developed an electrical equivalent circuit based on a simple parallel layer model well describing our impedance and interferometric results of porous alumina and those of others. Moreover, the model addresses the question of the electrically active area, enabling us to calculate specific parameters of the immobilized lipid bilayers. The obtained electrical parameters of the porous alumina layers indicated that a sensitive detection of lipid bilayers immobilized on the porous alumina surface is not feasible. Thus, we established a technique first described by Nielsch et al.[23] to thin out the barrier layer at the bottom of the pores, allowing us to sensitively detect lipid membranes covering the porous substrate. Insulating lipid membranes on the porous alumina substrates were achieved by two different strategies based on vesicle fusion, and electrical parameters of the resultant lipid membranes were obtained by means of equivalent circuit modeling.

Materials and Methods

Materials. Aluminum substrates (thickness 0.5 mm, purity 99.999%) and platinum wires (thickness 1 mm, purity 99.95%) were purchased from Goodfellow (Goodfellow Cambridge Limited, U.K.). 1-Palmitoyl-2-oleoyl-*sn*-glycero-3-[phospho-*rac*-(1-glycerol)] (POPG), 1,2-dipalmitoyl-*sn*-glycero-3-phosphothioethanol (DPPTE), and 1,2-dioleoyl-*sn*-glycero-3-phosphocholine (DOPC) were purchased from Avanti Polar Lipids (Alabaster, AL). Cholesterol was obtained from Sigma, and soybean asolectin, from Fluka. Bis-Tris was purchased from Sigma. Orthophosphoric acid (85%), sulfuric acid (95−97%), oxalic acid, and chromium(VI) oxide dihydrate were from Merck. The water used was ion-exchanged and Millipore-filtered (Millipore, France).

Electrical Impedance Spectroscopy (EIS). Porous alumina substrates and lipid membrane covered porous alumina were investigated using electrical impedance spectroscopy. The complex electrical impedance $Z(\omega)$ is determined by the ratio between the applied voltage $U(\omega)$ and the measured current response $I(\omega)$ of the sample as a function of frequency (eq 1):

$$Z(\omega) = \frac{U(\omega)}{I(\omega)} = |Z(\omega)| \exp[i\varphi(\omega)] \qquad (1)$$

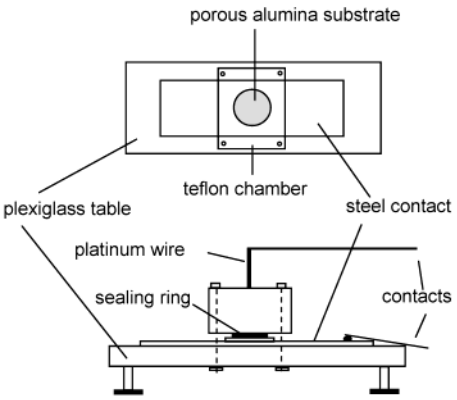

Figure 1. Schematic drawing of the experimental setup used for impedance analysis of porous alumina.

Impedance spectra were recorded with the impedance analyzer from Solartron Instruments (SI 1260, Farnborough, U.K.). The frequency was varied between 0.1 and 10^6 Hz, while the applied voltage amplitude was set to 30 mV (rms). A two electrode configuration was used, in which the porous alumina substrate, placed in a Teflon chamber sealed by an O-ring, served as working electrode, while a platinized platinum wire in the electrolyte solution served as counter electrode. Electrical contact of the aluminum was accomplished by a slightly larger steel disk contacting the aluminum from the back-side (Figure 1). The geometric, electrolyte-exposed area of the porous alumina sample was 0.3 and 0.8 cm^2, respectively. All measurements were performed in 0.1 M Na_2SO_4 or 10 mM Bis-Tris, 10 mM Na_2SO_4, pH 5.5. For data representation and evaluation, the absolute value of the impedance $|Z(\omega)|$ and the phase difference between voltage and current $\varphi(\omega)$ were used. Data analysis was performed using different equivalent circuits as outlined below using the program ZView2.

Interference Reflectance Spectra. Interference reflectance spectra of porous alumina were recorded by using an Ocean Optics S 1000 spectrometer (Dunedin, FL) fitted with a bifurcated fiber optic probe. A tungsten light source was focused onto the center of the porous alumina surface with a spot size of approximately 1−2 mm. Spectra were recorded in the wavelength range of 400−900 nm. Illumination and detection of light were performed along the surface normal. Data acquisition and evaluation were achieved with a self-written program in LabView 6.0. Extraction of the effective optical thickness from the interference pattern was accomplished by Fourier analysis and curve fitting of the reflectance spectra considering eq 2:

$$m\lambda = 2n_{\text{eff}}d \qquad (2)$$

where m is the fringe order, λ is the wavelength, n_{eff} is the effective refractive index, and d is the thickness of the layer.

Preparation of Porous Alumina Substrates. High purity aluminum foils were first annealed for 3 h at 500 °C under a nitrogen atmosphere to remove mechanical stresses and recrystallize the sample to increase grain boundaries. To smooth the surface, the aluminum substrates (2 × 2 cm^2) were electropolished four times in a sulfuric/phosphoric acid/water (2:2:1) mixture at 70 °C for 40 s and thoroughly rinsed with water directly after removal of the acidic solution. Nonordered pores were obtained by a one-step anodization process in 0.3 M oxalic acid at 2 °C and 40 V for several hours. To control the anodization process, the current was continuously recorded. The

porous substrates display pores with pore diameters of (20 ± 5) nm with a surface porosity of (16 ± 2)% obtained from scanning electron microscopy after gold coating. Hexagonally ordered pores were obtained by a two-step anodization process according to Gösele and co-workers.[23−25] First, aluminum was anodized in 0.3 M oxalic acid at 2 °C and 40 V for several hours. Second, the anodically etched porous alumina layer was removed by incubating the sample in a stirred acidic chromium-(VI) oxide solution at 70 °C for several hours followed by a second anodization step conducted under the same conditions as those for the first one. Due to prestructuring of the surface during the first anodization process, pores that are formed in the second step are hexagonally ordered with pore sizes of (50 ± 5) nm and a surface porosity of (50 ± 10)%. Pore depth depends on etching time and is reported to be about 1−2 μm/h.[23−26]

To decrease the thickness of the barrier layer at the bottom of the pores, an exponentially decreasing dc voltage starting at 40 V and stopping at 50 mV with a time constant of $\tau = 40$ min was applied to the porous alumina substrate in 0.3 M oxalic acid at 2 °C. Afterward, the porous alumina samples were immediately rinsed with water.

Gold coating of the upper surface of the porous alumina substrates was achieved by gold sputtering (25 nm) using a sputter coater with a thickness control unit (Cressington sputter coater 108 auto, Cressington mtm20, Elektronen-Optik-Service GmbH, Dortmund, Germany). Surfaces were cleaned before lipid membrane preparation using a plasma cleaner (Harrick Scientific Corporation, New York, NY).

Preparation of Planar Barrier Layers. Planar barrier layers were prepared according to two different procedures. For both methods, aluminum was first electropolished as described above. In the first method, the anodization protocol was started as described above but was stopped immediately after the current minimum had been reached. The obtained planar barrier layer is supposed to have the same thickness as that of the barrier layer at the pore bottoms of porous alumina. In the second method, aluminum was anodized at room temperature in 0.3 M boric acid, while the current was limited to 0.1 A. The current decreases exponentially to zero in about 60−120 s, denoting the end of anodization. The resulting thickness of the planar barrier layer is 1.2−1.7 nm/V.[27] After anodization, the samples were immediately rinsed with water.

Preparation of Lipid Bilayers on Porous Alumina Substrates. Lipid bilayers were prepared by spreading and fusing unilamellar vesicles onto porous alumina. We followed two different strategies: (i) adhesion and spreading of negatively charged giant unilamellar vesicles, applying a positive bias potential, and (ii) self-assembly of large unilamellar vesicles containing lipids with a thiol anchor onto gold covered porous alumina substrates.

(i) Giant unilamellar vesicles were prepared from a lipid mixture composed of 70 wt % asolectin, 25 wt % POPG, and 5 wt % cholesterol. Lipids were mixed in appropriate proportions from stock solutions in chloroform and dried at the bottom of glass test tubes under a stream of nitrogen and in a vacuum for 3 h. The lipid film was rehydrated by the addition of water at room temperature for several hours, resulting in a lipid concentration of 0.1−0.2 mg/mL. Giant unilamellar vesicles are formed due to electrostatic repulsion between the negatively charged lipid bilayers, and they were stable for several weeks.[28] To control the formation of giant unilamellar vesicles, 1 mol % β-Bodipy was added to the lipid films, and vesicles were observed by fluorescence microscopy. Resulting observable vesicles exhibited diameters between 1 and 30 μm. Vesicle spreading was achieved by applying a voltage of +100 mV to the alumina substrate relative to a platinum wire for several hours. Afterward, the surface was rinsed several times with water to remove intact vesicles from the solution and surface.

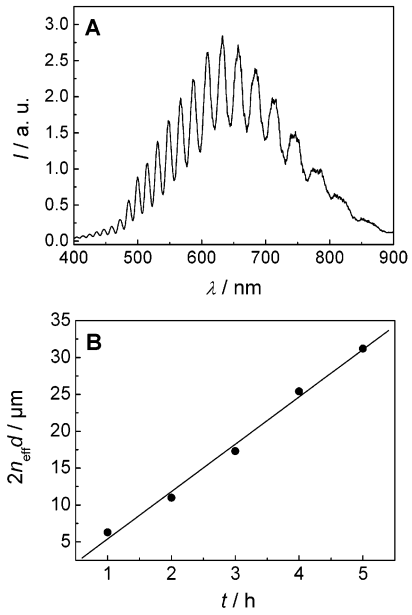

Figure 2. (A) Interference reflectance spectrum of nonordered porous alumina etched in 0.3 M oxalic acid at $T = 2$ °C and $U = 40$ V for 3 h. (B) Effective optical thickness vs anodization time. The solid line is the result of a linear regression with a slope of 6.4 μm/h.

(ii) 1,2-Dipalmitoyl-*sn*-glycero-3-phosphothioethanol (DPPTE) and 1,2-dioleoyl-*sn*-glycero-3-phosphocholine (DOPC) were mixed in appropriate proportions from stock solutions in chloroform, dried on the bottom of glass test tubes with a stream of nitrogen, desiccated under vacuum for 3 h, and rehydrated by the addition of outgassed 10 mM Bis-Tris, 10 mM Na_2SO_4, pH 5.5 at 50 °C for 30 min. The lipid suspension was vortexed several times, and large unilamellar vesicles were prepared by the extrusion method (Miniextruder Liposofast, Avestin, Ottawa, Ontario, Canada) using a polycarbonate membrane of 400 nm pore size. Bilayer preparation was achieved by incubating the vesicle suspension (1 mg/mL) with the gold coated porous alumina substrate overnight at 50 °C. Afterward, the sample was rinsed with buffer solution several times in order to remove vesicles attached to the lipid bilayer and from solution.

Results

Interference Reflectance Analysis of Porous Alumina. Porous alumina exhibits a Fabry−Perot fringe pattern when illuminated with white light (Figure 2). A Fabry−Perot fringe pattern is created by multiple reflections of illuminated white light on the air−porous alumina and porous alumina−aluminum interfaces. Interference reflectance spectra were monitored for porous alumina substrates in air obtained after different anodization times, and the effective optical thicknesses $2n_{eff}d$ were obtained by Fourier analysis and curve fitting of the reflectance spectra (Figure 2). The effective optical thickness increases linearly with increasing anodization time. It is assumed that the effective refractive index n_{eff} remains constant during the etching procedure, while the thickness d of the porous layer increases continuously. Using the effective medium approximation according to Bruggeman developed for cylindrical pores (eq 3),

SCHEME 1: Schematic Drawing of the Alumina Substrates and Terminology: (A) Porous Alumina Substrate; (B) Planar Barrier Layer

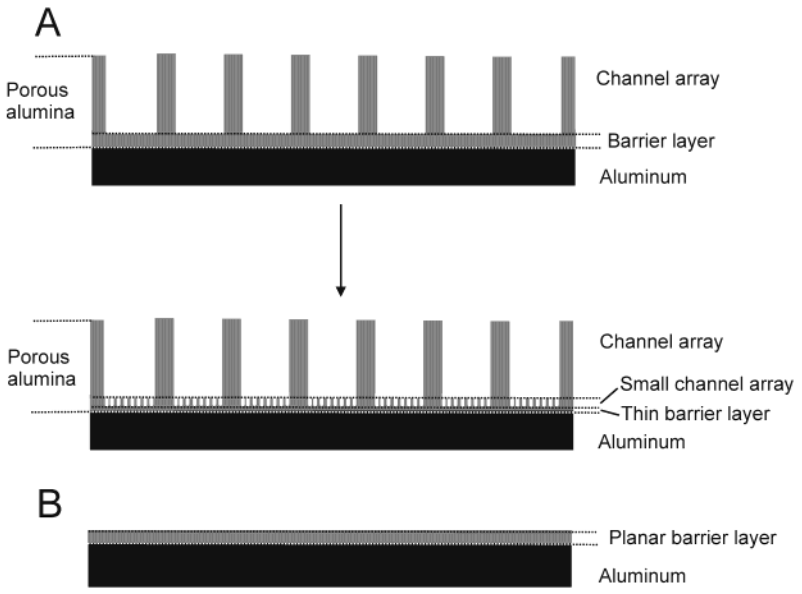

an effective refractive index n_{eff} of the porous alumina layer can be calculated:[29]

$$\frac{n_{air}^2 - n_{eff}^2}{n_{air}^2 + n_{eff}^2} p + \frac{n_{Alox}^2 - n_{eff}^2}{n_{Alox}^2 + n_{eff}^2}(1 - p) = 0 \qquad (3)$$

The refractive index of air is $n_{air} = 1.003$, and that of aluminum oxide is $n_{Alox} = 1.77$ ($\lambda = 550$ nm). The porosity p for nonordered, as-etched pores is $p = 0.16$, which was determined from scanning electron microscopy images assuming ideal cylindrical pores. Taking these values into account, the effective refractive index of the porous alumina layer is calculated to be $n_{eff} = 1.63$. From the obtained slope (Figure 2), a linear pore growth rate of 2.0 μm/h is then calculated, which agrees very well with those reported by others.[23−26]

Impedance Analysis of Porous Alumina. A prerequisite for the evaluation of impedance spectra of lipid membrane covered porous alumina is a comprehensive understanding of the impedance behavior of porous alumina itself. Various electrical models have been discussed in the literature to model the electrical properties of porous alumina.[12−16] To clear up whether the channel array (Scheme 1A) of the porous alumina contributes to the overall impedance, porous aluminas with different layer thicknesses were prepared and impedance spectra were taken. Independent of the anodization time, which results in an increased thickness of the channel array (see Figure 2B), the same impedance spectra (Figure 3) were obtained, providing clear evidence that the thickness of the channel array does not contribute to the overall impedance of porous alumina, particularly the frequency dependent part given by the capacitance. To model this electrical behavior of porous alumina by an equivalent circuit, the two different layers, the barrier layer at the bottom of the pores and the channel array composed of Al_2O_3 and electrolyte, are treated separately. The channel array can be ascribed by a parallel layer model,[30] in which Al_2O_3 and electrolyte are stacked across the electrode, which is composed of aluminum and the barrier layer. For this parallel layer model, the complex conductivity ψ_j (eq 4)

$$\psi_j = \sigma_j + i\omega\epsilon_j \qquad (4)$$

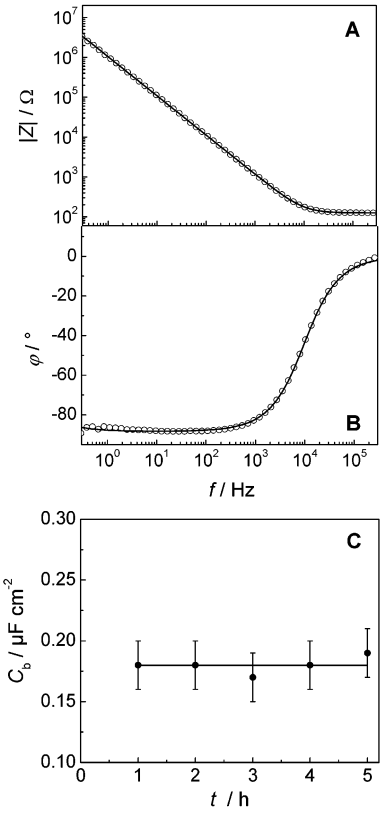

Figure 3. (A and B) Impedance spectra of nonordered porous alumina in 100 mM Na_2SO_4. The result of fitting the parameters of equivalent circuit 1a is given as a solid line. $C_b = 0.20$ μF/cm^2; $R_b > 10^7$ Ω cm^2. (C) Specific capacitances C_b of porous alumina obtained after different anodization times.

with σ_j being the conductivity and ϵ_j being the permittivity of phase j, follows a linear mixing rule of the two layers (eq 5):

$$\psi_{eff} = \chi_{Alox}\psi_{Alox} + \chi_{el}\psi_{el} \qquad (5)$$

χ_{Alox} and χ_{el} are the volume fractions of Al_2O_3 and electrolyte, respectively.

SCHEME 2: Equivalent Circuits Used throughout This Study To Model the Impedance Data

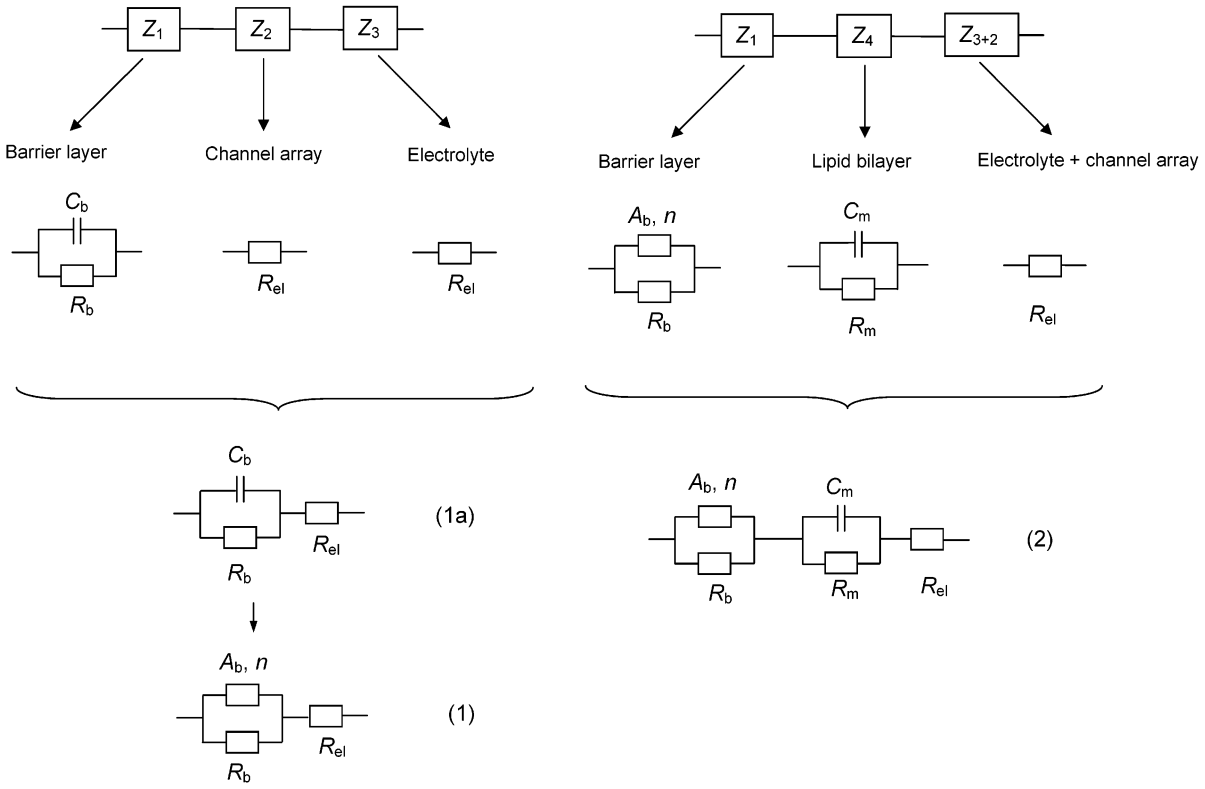

This treatment results in an equivalent circuit composed of two parallel *RC*-elements, which transforms into one *RC*-element with a conductivity σ_{eff} (eq 6),

$$\sigma_{eff} = \chi_{Alox}\sigma_{Alox} + \chi_{el}\sigma_{el} \quad (6)$$

and a permittivity ϵ_{eff} (eq 7),

$$\epsilon_{eff} = \chi_{Alox}\epsilon_{Alox} + \chi_{el}\epsilon_{el} \quad (7)$$

As $\sigma_{el} \gg \sigma_{Alox}$ and $\epsilon_{el} \gg \epsilon_{Alox}$, σ_{eff}, ϵ_{eff} and thus G_{eff} and C_{eff} are determined by the properties of the electrolyte. Hence, the channel array can be represented by a small ohmic resistance R_{el} that merges with the bulk electrolyte resistance. This is consistent with the observation that, independent of the thickness of the channel array, the same impedance spectrum was obtained. The barrier layer can be modeled by a capacitance C_b representing the dielectric behavior of Al_2O_3 in parallel with an ohmic resistance R_b representing the ion conductance across the barrier layer. Equivalent circuit 1a depicted in Scheme 2 combines the electrical elements of the channel array, the barrier layer, and the electrolyte. Fitting the parameters of the equivalent circuit to the impedance spectra results in very good agreement (Figure 3A and B).

As the electrical properties of the porous alumina remain constant during the anodization process and as the electrical properties are solely determined by the barrier layer, it can be concluded that the thickness of the barrier layer is constant and independent of the anodization time. Even more important is the result that the measured active area of porous alumina is only determined by the geometric area of the barrier layer. Taking this area into account, which is determined by the area surrounded by the O-ring, a specific capacitance of $C_b = (0.20 \pm 0.03)$ μF/cm^2 and a resistance $R_b > 10^7$ Ω cm^2 can be calculated independent of anodization time (Figure 3C).

The result that only the barrier layer is measured by impedance analysis and that the channel array does not contribute to the overall impedance was corroborated by investigating planar barrier layers (Scheme 1B) with the same thickness as that of the barrier layer at the bottom of the pores of a porous substrate and with the same geometric area.[16] The obtained impedance spectra were almost identical with the same electrical parameters obtained for planar barrier layers and for porous layers (data not shown). This result confirms the hypothesis of solely measuring the barrier layer of the porous alumina.

As the specific capacitance of the barrier layer C_b is much smaller than that of a solid supported lipid bilayer, which is typically in the range 0.6−1.0 μF/cm^2,[2,7,31−36] and the barrier layer resistance R_b is larger than 10^7 Ω cm^2, a lipid bilayer on top of the porous alumina substrate could hardly be detected.

To overcome this problem, we have established a method to modify the electrical behavior of the barrier layer by decreasing the thickness of the barrier layer and, as a consequence, increasing its specific capacitance (Scheme 1A). An exponentially decaying voltage is applied to the as etched porous alumina, starting from 40 V and eventually stopping at 50 mV with a time constant of $\tau = 40$ min. The process was followed by impedance spectroscopy. As expected for an effective thinning of the barrier layer, the impedance of the porous alumina substrate changes considerably dependent on the applied final voltage (Figure 4). Fitting the parameters of equivalent circuit 1a depicted in Scheme 2 to the data indicates that the capacitance of the barrier layer increases, while its resistance decreases. However, it turned out that with decreasing voltage the agreement between impedance data and fit became less perfect. Deviations from an ideal impedance behavior are often treated by using the constant phase element (cpe) instead of an ideal capacitance. The origin of a cpe-behavior is discussed controversially. It is generally believed that it originates from

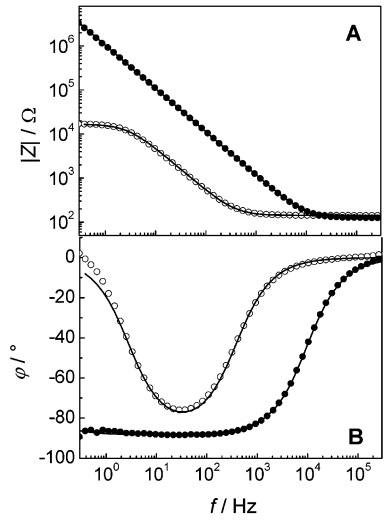

Figure 4. Impedance spectra before (●) and after (○) the application of an exponentially decaying voltage down to 1 V during the etching procedure. The parameters of equivalent circuit 1 were fitted to the data with the following results: (●) $A_b = 0.20$ μF/cm^2, $n = 0.99$, $R_b > 10^7$ Ω cm^2; (○) $A_b = 4.6$ μF/cm^2, $n = 0.97$, $R_b = 13$ kΩ cm^2. The solid lines are the results of the fitting procedure.

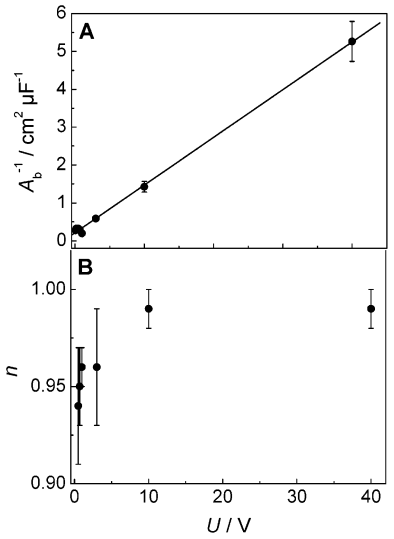

Figure 5. (A) Plot of A_b^{-1} vs the applied voltage U. The slope was determined to be $m = 0.126$ cm^2 μF^{-1} V^{-1}. (B) Plot of n vs the applied voltage.

a distribution in the current density along the electrode surfaces as a result of surface inhomogeneity. This is inferred from the analogy with the behavior of porous electrodes, which has been extensively discussed by de Levie.[21] To account for the observed deviation of the thinned porous alumina substrates in our case, we introduced the cpe-element instead of the capacitance C_b. In contrast to the fitting results obtained by using equivalent circuit 1a, those achieved by using equivalent circuit 1 exhibit good agreement between data and fit. The result of the fitting procedure is shown in Figure 4.

As dendritelike pore structures at the barrier layer emerge during the thinning process, only the remaining thin barrier layer at the bottom of the small channel area (Scheme 1A) contributes to the impedance behavior of the porous alumina substrate, in accordance with the theoretical treatment of the porous alumina based on the parallel layer model described above. Again, the channel array of the porous alumina and the small channel array emerging during the thinning process at the barrier layer are not resolved by impedance spectroscopy, as they are indistinguishable from the bulk electrolyte. Thus, the active area of the thinned porous alumina substrate is again the geometric area of the barrier layer. The area-specific values for A_b together with the exponent n as a function of the applied voltage are given in Figure 5. n decreases nonlinearly from 0.99 in the range 10−40 V to 0.96−0.90 at 100−50 mV, while A_b^{-1} depends in a linear fashion on the applied voltage. As a first approximation, the values for A_b can be treated as a capacitance C_b, as n is still close to one, indicating a capacitive behavior of the barrier layer. Assuming a plate condenser for the barrier layer with a dielectric constant of $\epsilon_{Alox} = 9.0$, one can calculate the thickness of the barrier layer at each applied voltage. The slope of the plot in Figure 5A then translates into a barrier layer thinning rate of 1 nm/V. This agrees very well with the reported value for barrier layer thicknesses of 1.3 nm/V and corroborates our model and approach.[23]

When the as prepared porous alumina substrates are stored in an aqueous solution, the electrical parameters are altered. A_b only slightly decreases, while R_b increases considerably with time. After 3 h of storing the porous alumina substrates in 0.1 M Na_2SO_4, no further changes in the electrical parameters were detected and equilibrium was reached. To ensure that the electrical parameters always reach their equilibrium values, all porous alumina substrates were soaked in aqueous solution overnight. During the incubation in aqueous solution, a slight increase in barrier layer thickness occurs, resulting in a slightly decreased A_b-value and an increased R_b-value. The final values for A_b were between 4 and 6 μF/cm^2, and they were always constant for one prepared alumina sample. The final values for R_b varied between 3×10^4 and 5×10^6 Ω cm^2. The thinning process not only results in a decreased barrier layer thickness but also widens the pores up to 2−5 nm, leading to an increased surface porosity by ∼2−5%.

Fusion of Giant Liposomes on Nonordered Porous Substrates. The preparation of lipid bilayers on porous surfaces starting from giant unilamellar vesicles allows, in principle, the formation of single lipid bilayers suspending the pores of the porous substrate, as these vesicles are excluded from the pores due to their size, which exceeds the pore size by at least a factor of 50. In a first set of experiments, porous alumina was coated with a thin gold layer providing the substrate for chemisorption of 3-mercaptoethylamine. At pH 5.5, this chemisorbed monolayer is positively charged so that negatively charged giant liposomes adhere to the surface and might spread at high adhesion forces to form planar bilayers.[35] Impedance spectra were taken before and after incubation of the surface with giant liposomes. After incubation, no change in the impedance of the system was obtained, indicating that the vesicles did not form an insulating surface-attached planar bilayer. In a different set of experiments, noncoated porous alumina was used and incubated with negatively charged giant liposomes while applying a voltage of +100 mV for 16 h. Again, impedance spectra were taken before and after the incubation process. After incubation, the impedance spectrum was significantly altered, indicating the formation of an insulating lipid layer (Figure 6). Control experiments, in which giant liposomes were incubated with porous alumina without applying a potential, and those in which porous alumina was incubated in an aqueous solution while applying a voltage of +100 mV did not lead to an altered impedance response after the incubation process. Hence, we conclude that an insulating lipid bilayer has been formed on the porous alumina surface under these conditions. To evaluate the measured impedance spectra, a model providing a mathematical expression for the electrical response of the system is required. In addition to the porous alumina, whose impedance

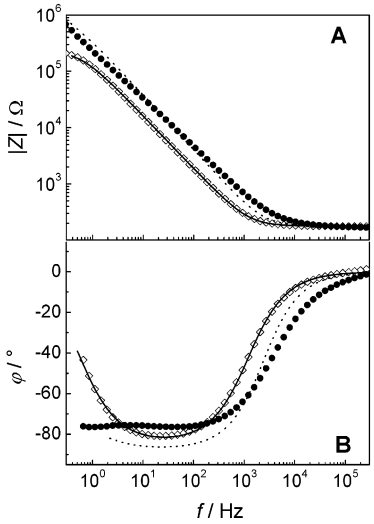

Figure 6. Impedance spectra of a nonordered porous alumina substrate before (◇) and after (●) incubation with giant liposomes while applying a voltage of +100 mV for 16 h. (◇) Equivalent circuit 1 was used to model the impedance spectra of the porous alumina substrate. The solid line is the result of the fitting procedure with the following values: $A_b = 4.2\ \mu F/cm^2$, $n = 0.94$, $R_b = 71\ k\Omega\ cm^2$. (●) Equivalent circuit 2 was used for data evaluation. The parameters of the porous alumina were kept constant during the fitting procedure. The result of the fitting routine is given as dotted line with $C_m = 2.4\ \mu F/cm^2$. R_m was not defined in the impedance spectra.

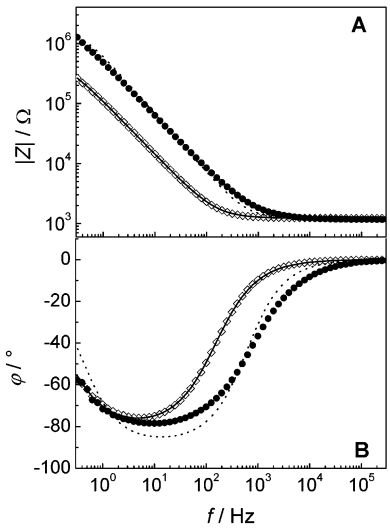

Figure 7. Impedance spectra of a nonordered gold covered porous alumina substrate before (◇) and after (●) incubation with DPPTE/DOPC (72:28) unilamellar vesicles (400 nm nominal diameter) overnight at 50 °C. (◇) Equivalent circuit 1 was used to model the impedance spectra of the porous alumina substrate. The result of the fitting procedure is given as a solid line with the following parameters: $A_b = 5.9\ \mu F/cm^2$, $n = 0.89$, $R_b = 207\ k\Omega\ cm^2$. (●) Equivalent circuit 2 was used for data evaluation. The parameters of the porous substrate were kept constant during the fitting procedure. The result of the fitting routine is shown as dotted line leading to a membrane capacitance of $C_m = 0.99\ \mu F/cm^2$ and a resistance of $R_m = 4 \times 10^5\ \Omega\ cm^2$.

response is modeled by equivalent circuit 1 depicted in Scheme 2, additional electrical elements have to be added to the equivalent circuit to account for the insulating lipid layer. The standard and most simple equivalent circuit of a lipid layer is composed of a parallel connection of a resistance R_m and capacitance C_m. Combining the equivalent circuit of the lipid bilayer with that representing porous alumina results in equivalent circuit 2 in Scheme 2. Fitting this simple equivalent circuit to the data reveals only limited agreement between the data and the model (Figure 6) with a specific capacitance value of 2.4 $\mu F/cm^2$. The membrane resistance was not defined in the impedance spectrum. During the fitting routine, the parameters of the porous alumina substrate were kept constant, as it is assumed that they do not change during the incubation process, which was experimentally verified by the control experiments.

Fusion of DPPTE-Containing Vesicles on Nonordered Porous Substrates. In a second set of experiments, we used vesicles that are known to chemisorb onto gold surfaces, resulting in almost defect free planar lipid bilayers. In general, vesicles were composed of 1,2-dipalmitoyl-*sn*-glycero-3-phosphothioethanol (DPPTE) and 1,2-dioleoyl-*sn*-glycero-3-phosphocholine (DOPC). To find the lipid mixture providing the best insulating planar lipid bilayers by vesicle spreading and fusion, vesicles composed of different mole fractions of DPPTE/DOPC were incubated with planar gold surfaces and investigated by impedance spectroscopy. It turned out that at least 50 mol % DPPTE is required for the formation of insulating planar lipid bilayers on gold, indicated by specific capacitances = (1.0 ± 0.2) $\mu F/cm^2$ and resistances > $10^7\ \Omega\ cm^2$. This optimized system was transferred to porous alumina. Nonordered porous alumina substrates were coated with a thin gold layer on top of the surface, ensuring a selective functionalization of the upper surface. These alumina substrates were incubated with a vesicle suspension composed of DPPTE/DOPC (72:28). To exclude vesicles from the pores, the nominal vesicle size was chosen to be 400 nm, which exceeds the pore size by a factor of 20. The incubation process resulted in a significant change in the impedance spectrum compared to the spectra of gold covered neat porous alumina taken prior the incubation process (Figure 7). As a control, impedance spectra of porous substrates incubated in pure buffer and in DOPC vesicle suspensions at 50 °C were taken. Only very slight changes in the impedance spectra were observed after incubation of the substrates in pure buffer and DOPC vesicle suspensions, respectively. These results indicate that the obtained changes in the impedance spectra can be attributed to the formation of an insulating lipid bilayer on the porous matrix. Fitting the parameters of equivalent circuit 2 to the obtained data, while keeping the parameters of the porous alumina substrate constant results in moderate agreement between the data and the fit. In this case, the obtained specific capacitance of 0.99 $\mu F/cm^2$ agrees with the expected value of (1.0 ± 0.2) $\mu F/cm^2$ for a solid supported membrane obtained from DPPTE/DOPC vesicle spreading and fusion on gold. This capacitance value is therefore indicative of a high surface coverage with bilayers with respect to planar gold electrodes as a reference.

Fusion of DPPTE-Containing Vesicles on Ordered Porous Substrates. The experiments described above clearly demonstrate that insulating lipid bilayers on porous alumina can be obtained. To gain a larger porosity and a less rough surface, we next used ordered pores instead of nonordered pores. The surface porosity of the ordered porous material is about 50% compared to that of nonordered porous alumina, which only exhibits a porosity of around 20%. An impedance spectrum of an ordered porous alumina substrate after the thinning process is depicted in Figure 8. The parameters of equivalent circuit 1 shown in Scheme 2 are fitted to the data, which results in an A_b-value of 7.7 $\mu F/cm^2$, slightly larger than those obtained for nonordered pores after the thinning process. Also the value for *n*, which was determined to be 0.86, is smaller than that of nonordered pores. Lipid vesicles composed of DPPTE/DOPC (72:28) obtained according to the extrusion method with polycarbonate membranes of 400 nm were incubated with the

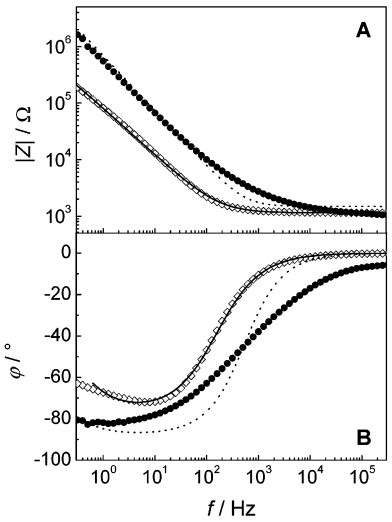

Figure 8. Impedance spectra of a gold covered ordered porous alumina substrate before (◇) and after (●) incubation with DPPTE/DOPC (72:28) unilamellar vesicles (400 nm nominal diameter) overnight at 50 °C. (◇) Equivalent circuit 1 was used to model the impedance spectra of the porous alumina substrate. The solid line is the result of the fitting routine with the following values: $A_b = 7.7\ \mu F/cm^2$, $n = 0.86$, $R_b = 146\ k\Omega\ cm^2$. (●) Equivalent circuit 2 was used for data evaluation. The values for the porous alumina substrate were kept constant during the fitting routine. The dotted line is the result of the fitting procedure with $C_m = 0.9\ \mu F/cm^2$. R_m was only poorly defined in the impedance spectra.

gold covered porous alumina substrate, and impedance spectra were again taken (Figure 8). Even without data evaluation it is evident that incubation of porous alumina with the vesicle suspension results in a significant alteration of the impedance spectrum compared to that obtained prior to the incubation process. Control experiments done at ordered porous substrates incubated at 50 °C in buffer solution and in DOPC vesicle suspensions, respectively, again lead to only minor changes in the impedance spectra. Equivalent circuit 2 was fitted to the obtained impedance data, leading to a specific capacitance of 0.9 $\mu F/cm^2$. However, as can be seen from the fitting results, the agreement between data and fit is only limited. Impedance spectra were taken over a period of more than 30 h without any detectable alteration.

Discussion

To sensitively investigate the electrical properties of lipid membranes immobilized onto porous alumina substrates, first the material itself needs to be thoroughly characterized and its electrical behavior modified. Porous alumina substrates were characterized by means of interferometry and electrical impedance spectroscopy. Interferometric measurements of porous alumina samples prepared at different anodization times revealed a linear dependence of the effective optical thickness on anodization time. This result is consistent with that observed by Vereecken and co-workers.[16] By means of ellipsometry, they observed a linear increase in porous alumina film thickness dependent on anodization time. This result validates our setup of preparing porous alumina substrates. To garner information about the electrical behavior of porous alumina, electrical impedance spectroscopy proved to be very useful.[12−16,37] Though several equivalent circuits are available in the literature to model the impedance response of porous alumina, none of them addresses the question of the active electrically measured area. However, to evaluate the electrical parameters of a lipid bilayer attached to the top of the porous alumina substrate, the active area needs to be known to calculate area independent specific electrical parameters of a lipid bilayer. From the impedance spectra of planar barrier and porous alumina layers recorded at different anodization times, it is clearly evident that only the barrier layer at the bottom of the pores is detected by impedance analysis within the observed frequency regime. The same conclusion was drawn by De Laet et al.[16] To model our impedance data, we used an equivalent circuit, which combines the electrical behavior of the channel array, based on a parallel layer model,[30] and the barrier layer of the porous alumina. Moreover, in this model, the active measured area, which is the geometric area of the porous alumina surface, is unambiguously defined. It should be mentioned that our results and those of De Laet et al.[16] are in contrast to those of Hitzig et al.[14] They proposed that both the channel array and the barrier layer are detected by electrical impedance spectroscopy and that the two oxide layers are distinguishable. Hitzig et al.[14] investigated porous alumina substrates with different layer thicknesses and found that the capacitance of the barrier layer remains constant, while the resistance of the channel array increases and its capacitance decreases with increasing layer thickness.

Fitting the parameters of equivalent circuit 1a (Scheme 2) results in a very good agreement between data and fit and leads to specific barrier layer capacitance values of $C_b = (0.20 \pm 0.03)\ \mu F/cm^2$ and specific resistances $R_b > 10^7\ \Omega\ cm^2$ for the porous alumina substrates. These values are in good agreement with those reported by Hoar and Wood,[12] who found barrier layer capacitances $= 0.47\ \mu F/cm^2$ and resistances $> 10^7\ \Omega\ cm^2$. They also used the solution exposed geometric area given by the sealing ring, so that their calculated specific parameters can be compared to our values. In general, in most publications the area that is used to calculate specific parameters is not explicitly defined, so that a comparison is difficult. Assuming that the solution exposed geometric area is used, Mansfeld and Kendig[13] reported a capacitance value for the barrier layer of $C_b = 0.5\ \mu F/cm^2$. De Laet et al.[16] applied a constant phase element instead of a capacitance to represent the barrier layer, obtaining $A_b = 0.94-1.03\ \mu F/cm^2$ and $n = 0.94-0.95$.

To sensitively detect a lipid bilayer with a specific capacitance of roughly 1 $\mu F/cm^2$ on top of the porous substrate, capacitance values of the porous alumina substrates must be considerably increased. A thinning procedure forming dendrite like structures at the barrier layer, first described by Nielsch et al.,[23] was applied, and for the first time impedance spectra were taken at different stages of this process. It turned out that with decreasing voltage the agreement between data and fit became less perfect by using equivalent circuit 1a. This might be a result of the formation of dendritelike structures at the barrier layer. To account for this deviation from an ideal capacitive behavior, we replaced the capacitance C_b in the equivalent circuit by a constant phase element (cpe).[37] Fitting the parameters of this modified equivalent circuit to the data led to a very good agreement. Interestingly, the value for n decreases with decreasing voltage. Though the origin of the cpe-behavior has not been well understood and is discussed controversially in the literature, there is some evidence that electrode roughness contributes to this behavior.[17−20] The decrease in n might reflect the microstructure of the barrier layer and could be used as a semiquantitative indicator for its increasing inhomogeneity with decreasing voltage.

However, as n typically ranges between 0.99 and 0.90 and is, thus, still close to one, the parameter A_b can be regarded as a capacitance as a first approximation. The successful thinning of the barrier layer can be deduced from the fact that the

parameter A_b increases considerably with decreasing voltage. A large A_b-value is a prerequisite for the sensitive electrochemical detection of a lipid bilayer on top of the porous alumina substrate.

For preparation of a lipid bilayer on the porous alumina substrate, vesicle spreading is a rather useful approach, as size exclusion together with a functionalization of the upper surface of the porous alumina substrate prevents the formation of lipid bilayers within the pores, as observed by Bourdillon and coworkers.[38,39] Moreover, vesicles allow for the insertion of membrane proteins, and the resultant planar lipid bilayers are solvent free. To induce vesicle adhesion and spreading via electrostatic interactions, the surface needs to be charged. This can be achieved by adsorbing charged molecules on the surface or by applying a voltage between a reference electrode and the surface, resulting in an accumulation of charges at the interface.[28,32] In the case of negatively charged giant liposomes, the formation of insulating planar bilayers was not observed on porous alumina surfaces, which were functionalized with a positively charged mercaptoethylamine. However, applying a voltage of +100 mV led to a significant change in the impedance spectra compared to those of bare porous alumina substrates. For data analysis, an equivalent circuit has been applied representing the porous alumina substrate and the lipid bilayer. The electrical parameters of the porous alumina substrate were determined before incubation with the vesicle suspension and kept constant during the fitting routine after bilayer formation. The assumption that the electrical parameters of porous alumina do not change during the incubation process seems to be justified, as no significant changes in the impedance behavior were observed in any of the control experiments.

The simplest and most well-known equivalent circuit representing a lipid bilayer is a parallel connection of a capacitance and a resistance.[7] Using this model, Wiegand et al.[7] reported membrane capacitances of 0.74−1.12 μF/cm^2 and resistances between 10^3 and 10^5 Ω cm^2 for lipid bilayers immobilized on semiconductor and gold surfaces. In particular, the membrane resistance strongly depends on pH, ionic strength, temperature, and the concentration of charged lipids and cholesterol, respectively. In general, lipid bilayers prepared from vesicle spreading and fusion on a hydrophilic surface exhibit slightly larger capacitances than those obtained from organic solvent[31] or vesicle fusion on a hydrophobic monolayer.[35,40] For example, lipid bilayers composed of *N*,*N*-dimethyl-*N*,*N*-dioctadecylammonium bromide immobilized on 3-mercaptopropionic acid modified gold electrodes typically exhibit membrane capacitances of about 1.0−1.1 μF/cm^2,[2,36] while fusion of a DMPG/DMPE mixture on a positively charged mercaptoethylamine monolayer results in a specific capacitance of 0.9 μF/cm^2.[35] The larger capacitances are discussed in terms of incomplete vesicle fusion, leading to defect structures within the bilayer. The increased number of defects and thus water within the bilayer leads to a larger overall dielectric constant. Fromherz et al.[41] had overcome this problem by touching one single giant vesicle to the open gate of a field-effect transistor. The lipid bilayer kept its continuous shape without rupturing, and it adhered onto the cationic polylysine film due to electrostatic interaction. They obtained a capacitance of 0.7 μF/cm^2, since fusion of several vesicles is not required for bilayer formation. Purrucker et al.[33] were able to obtain lipid bilayers from vesicle fusion onto smooth silicon−silicon dioxide surfaces with low membrane capacitances of 0.7 μF/cm^2. Here, the low roughness of the surface presumably favors fewer defects within the bilayer. In our case, the obtained capacitances can be best compared with the cases of lipid bilayers obtained from spreading and fusion of charged vesicles on a charged surface with typical specific capacitances of 0.9−1.1 μF/cm^2. Capacitances obtained from lipid bilayers achieved by fusing giant liposomes onto porous alumina are 2.4 μF/cm^2 and are thus at least a factor of 2 larger than those obtained by vesicle fusion onto charged surfaces on gold surfaces. The larger capacitance indicates an incomplete surface coverage. The overall measured capacitance is the sum of the capacitances arising from the lipid bilayer with a dielectric constant of the hydrocarbon chains of 2.0−2.2 and the defects occupied by water with a dielectric constant of 80. According to this picture, one might find it useful to calculate the surface coverage Θ with bilayers by assuming a parallel combination of two capacitances reflecting the defect free bilayers, C_{bi} (0.7 μF/cm^2), and the defects, C_d (4 μF/cm^2), represented mainly by the barrier layer (eq 8):

$$\Theta = \frac{C_m - C_d}{C_{bi} - C_d} \tag{8}$$

C_m is the measured capacitance. The surface coverage for giant liposomes then amounts to roughly 50%.

Feder et al.[42] found that giant vesicles retain their original topology while spreading, but they flatten and exhibit fractal-like structures for moderately strong adhesion. If the attraction is too strong, vesicles burst; if it is too weak, no adhesion is observed due to the Helfrich steric repulsion. It is conceivable that not all giant liposomes adhere that strongly to the surface on which they spread and fuse to form planar lipid bilayers, which would lead to structural inhomogeneities and thus to defects within the lipid bilayer structure.

In a different approach starting from large unilamellar vesicles with a nominal diameter of 400 nm, the upper surface was coated with a thin gold layer, while lipid vesicles were used carrying thiol anchors to allow for chemisorption of the vesicles on the gold surface. By using 400 nm vesicles, the tendency of the vesicles to diffuse into the pores is low due to size exclusion, while there is a strong affinity toward the upper gold surface. To find an optimized system, vesicles composed of DPPTE and DOPC varying in the amount of DPPTE were incubated with planar gold electrodes and impedance spectra were taken. It turned out that at least 50 mol % DPPTE is required to obtain almost defect free planar lipid bilayers with capacitance values of (1.0 ± 0.2) μF/cm^2. The optimized system was transferred to nonordered porous alumina substrates with a surface porosity of around 20%. Data analysis revealed a capacitance of 0.99 μF/cm^2 using an equivalent circuit consisting of one parallel *RC*-circuit representing the electrical behavior of a lipid membrane. According to eq 8, the capacitance value translates into a surface coverage of Θ > 90%. The obtained capacitance on the porous surface is the same as that achieved on planar gold electrodes as a reference for high coverage. To increase the surface porosity and to obtain a more defined and less rough surface, we also used hexagonally ordered porous alumina substrates. Even though the porosity of ordered porous alumina substrates is significantly higher (50%) than that of nonordered pores (20%), a similar value of 0.9 μF/cm^2 for the membrane capacitance was obtained assuming equivalent circuit 2 shown in Scheme 2. The fact that the same capacitance was obtained for a lipid bilayer on nonordered and ordered pores—though the porosity of these two substrates is about 30% different—verifies further that not only are the pore columns of the channel array covered by a lipid bilayer but also the pores are membrane suspended.

Conclusion

We established a procedure to modify porous alumina, so that insulating lipid bilayers immobilized on the porous matrix can be investigated by means of impedance spectroscopy. By vesicle spreading techniques, insulating lipid membranes were formed on porous alumina, and the membranes were characterized by their electrical parameters. These membranes spanning the pores of the porous substrate will open up the avenue to nanocompartments separated by a semipermeable lipid membrane serving as containers for biochemical reactions. Experiments are underway to demonstrate that these model membranes are suited for the insertion of fully functional transmembrane proteins and the establishment of electrochemical and chemical gradients.

Acknowledgment. Funding by the DFG is gratefully acknowledged (STE 884/2-1 and 2-2). We thank K. Nielsch and A. Janshoff for fruitful discussions.

References and Notes

(1) Sackmann, E. *Science* **1996**, *271*, 43.
(2) Michalke, A.; Schürholz, T.; Galla, H.-J.; Steinem, C. *Langmuir* **2001**, *17*, 2251.
(3) Knoll, W.; Frank, C. W.; Heibel, C.; Naumann, R.; Offenhäusser, A.; Rühe, J.; Schmidt, E. K.; Shen, W. W.; Sinner, A. *Rev. Mol. Biotechnol.* **2000**, *74*, 137.
(4) Salamon, Z.; Tollin, G. *Biophys. J.* **1996**, *71*, 858.
(5) Majewski, J.; Wong, J. Y.; Park, C. K.; Seitz, M.; Israelachvili, J. N.; Smith, G. S. *Biophys. J.* **1998**, *75*, 2363.
(6) Sackmann, E.; Tanaka, M. *Trends Biotechnol.* **2000**, *18*, 58.
(7) Wiegand, G.; Arribas-Layton, N.; Hillebrandt, H.; Sackmann, E.; Wagner, P. *J. Phys. Chem. B* **2002**, *106*, 4245.
(8) Hillebrandt, H.; Wiegand, G.; Tanaka, M.; Sackmann, E. *Langmuir* **1999**, *15*, 8451.
(9) Müller, P.; Rudin, D. O. *Nature* **1967**, *213*, 603.
(10) Hennesthal, C.; Steinem, C. *J. Am. Chem. Soc.* **2000**, *122*, 8085.
(11) Hennesthal, C.; Drexler, J.; Steinem, C. *Chem. Phys. Chem.* **2002**, *10*, 885.
(12) Hoar, T. P.; Wood, G. C. *Electrochim. Acta* **1962**, *7*, 333.
(13) Mansfeld, F.; Kendig, M. W. *J. Electrochem. Soc.* **1988**, *135*, 828.
(14) Hitzig, J.; Jüttner, K.; Lorenz, W. J.; Paatsch, W. *J. Electrochem. Soc.* **1986**, *133*, 887.
(15) Van der Linden, B.; Terryn, H.; Vereecken, J. *J. Appl. Electrochem.* **1990**, *20*, 798.
(16) De Laet, J.; Terryn, H.; Vereecken, J. *Electrochim. Acta* **1996**, *41*, 1155.
(17) Diao, P.; Jiang, D.; Cui, X.; Gu, D.; Tong, R.; Zhong, B. *J. Electroanal. Chem.* **1999**, *464*, 61.
(18) Kerner, Z.; Pajkossy, T. *J. Electroanal. Chem.* **1998**, *448*, 139.
(19) Sadkowsky, A. *J. Electroanal. Chem.* **2000**, *481*, 222.
(20) Sadkowsky, A.; Motheo, A. J.; Neves, R. S. *J. Electroanal. Chem.* **1998**, *455*, 107.
(21) de Levie, R. *Electrochim. Acta* **1964**, *9*, 1231.
(22) Scheider, W. *J. Phys. Chem. B* **1975**, *79*, 127.
(23) Nielsch, K.; Müller, F.; Li, A.-P.; Gösele, U. *Adv. Mater.* **2000**, *12*, 582.
(24) Li, A.-P.; Müller, F.; Birner, A.; Nielsch, K.; Gösele, U. *J. Appl. Phys.* **1998**, *84*, 6023.
(25) Li, A. P.; Müller, F.; Birner, A.; Nielsch, K.; Gösele, U. *J. Vac. Sci. Technol. A* **1999**, *17*, 1428.
(26) Jessensky, O.; Müller, F.; Gösele, U. *Appl. Phys. Lett.* **1998**, *72*, 1173.
(27) Serebrennikova, I.; Vanysek, P.; Birss, V. I. *Electrochim. Acta* **1997**, *42*, 145.
(28) Schmidt, C.; Mayer, M.; Vogel, H. *Angew. Chem., Int. Ed.* **2000**, *39*, 3137.
(29) Bruggeman, D. A. G. *Ann. Phys. (Leipzig)* **1935**, *24*, 636.
(30) Macdonald, J. R. *Impedance Spectroscopy*; John Wiley & Sons: New York, 1987.
(31) Asaka, K.; Ottova, A.; Tien, H. T. *Thin Solid Films* **1999**, *354*, 201.
(32) Michalke, A.; Galla, H.-J.; Steinem, C. *Eur. Biophys. J.* **2001**, *30*, 421.
(33) Purrucker, O.; Hillebrandt, H.; Adlkofer, K.; Tanaka, M. *Electrochim. Acta* **2001**, *47*, 791.
(34) Raguse, B.; Braach-Maksvytis, V.; Cornell, B. A.; King, L. G.; Osman, P. D. J.; Pace, R. J.; Wieczorek, L. *Langmuir* **1998**, *14*, 648.
(35) Steinem, C.; Janshoff, A.; Ulrich, W.-P.; Sieber, M.; Galla, H.-J. *Biochim. Biophys. Acta* **1996**, *1279*, 169.
(36) Steinem, C.; Janshoff, A.; Galla, H.-J.; Sieber, M. *Bioelectrochem. Bioenerg.* **1997**, *42*, 213.
(37) Goeminne, G. T. H.; Vereecken, J. *Electrochim. Acta* **1995**, *40*, 479.
(38) Delrouyre, V.; Laval, J.-M.; Bourdillon, C. *J. Am. Chem. Soc.* **2001**, *123*, 9176.
(39) Marchal, D.; Boireau, W.; Laval, J. M.; Moiroux, J.; Bourdillon, C. *Biophys. J.* **1998**, *74*, 1937.
(40) Plant, A. L.; Gueguetchkeri, M.; Yap, W. *Biophys. J.* **1994**, *67*, 1126.
(41) Fromherz, P.; Kiessling, V.; Kottig, K.; Zeck, G. *Appl. Phys. A* **1999**, *69*, 571.
(42) Feder, T. J.; Weissmüller, G.; Zeks, B.; Sackmann, E. *Phys. Rev. E.* **1995**, *51*, 3427.